J. Am. Soc. Mass Spectrom. (2014) 25:1780–1787
DOI: 10.1007/s13361-014-0958-0

RESEARCH ARTICLE

Experimental Investigation of the 2D Ion Beam Profile Generated by an ESI Octopole-QMS System

Sarfaraz U. A. H. Syed,[1] Gert B. Eijkel,[1] Piet Kistemaker,[1] Shane Ellis,[1] Simon Maher,[2] Donald F. Smith,[1] Ron M. A. Heeren[1]

[1]FOM Institute AMOLF, Science Park 104, 1098 XG, Amsterdam, The Netherlands
[2]Department of Electrical Engineering and Electronics, University of Liverpool, Liverpool, L69 3GJ, UK

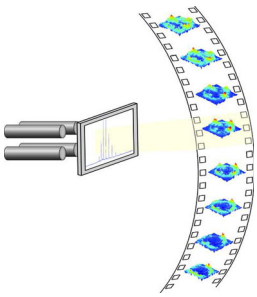

Abstract. In this paper, we have employed an ion imaging approach to investigate the behavior of ions exiting from a quadrupole mass spectrometer (QMS) system that employs a radio frequency octopole ion guide before the QMS. An in-vacuum active pixel detector (Timepix) is employed at the exit of the QMS to image the ion patterns. The detector assembly simultaneously records the ion impact position and number of ions per pixel in every measurement frame. The transmission characteristics of the ion beam exiting the QMS are studied using this imaging detector under different operating conditions. Experimental results confirm that the ion spatial distribution exiting the QMS is heavily influenced by ion injection conditions. Furthermore, ion images from Timepix measurements of protein standards demonstrate the capability to enhance the quality of the mass spectral information and provide a detailed insight in the spatial distribution of different charge states (and hence different *m/z)* ions exiting the QMS.

Key words: Quadrupole, Imaging MS, Ion transmission, Active pixel detector

Received: 5 April 2014/Revised: 8 June 2014/Accepted: 8 June 2014/Published Online: 12 August 2014

Introduction

Electrospray ionization (ESI) is one of the most widely used ionization methods for analysis of high molecular weight species in biological mass spectrometry [1]. ESI allows for ionization of analytes at atmospheric pressure and often result in the formation of multiply charged gas-phase ions [2]. It has been widely interfaced with different mass spectrometer (MS) instruments such as QMS; time-of-flight mass spectrometers (TOFMS), and Fourier transform ion cyclotron resonance mass spectrometers (FTICR-MS). Quadrupoles and octopoles are the most widely used ion guides for efficient transport of ions from low vacuum region to high vacuum regions.

Since the invention of the linear quadrupole by Wolfgang Paul and co-workers in the 1950s [3], many researchers have investigated the performance and behavior of the QMS by either experimental methods or numerical simulation techniques. Brubaker and Tuul, investigated the transmission efficiency and resolution of a QMS as a function of ion source exit aperture and frequency of excitation (f) [4]. It was concluded that higher resolution is obtained with small aperture size and higher frequency. Later, Dylla and Jarrell showed experimentally that by using an entrance aperture which spatially separates the radio frequency (rf) and direct current (DC) fringe fields in a QMS, transmission-resolution characteristics can be improved [5].

There have been many analytical predictions of the behavior of QMS. Few examples of analytical investigations include a detailed review of quadrupole gas analyzers by Batey in 1987. It was shown that the QMS behavior could be predicted by tracing ion motion through the mass filter [6]. Later, in 1993, Konenkov investigated the influence of fringing fields on the acceptance of a QMS in the separation mode of the intermediate stability region [7]. More recently, it was shown that fringe fields at the QMS entrance and exit will also affect ion paths, which have recently been modeled to a high degree of accuracy [8], where the theoretical predictions agree with experimental observations.

In the past, ion beam properties of QMS have also been investigated experimentally. Weaver and Mathers, in their work published in Dynamic Mass Spectrometry No. 5 (1978) pages 41–54, Chapter 3 "Modulation Techniques Applied to Quadrupole Mass Spectrometry" [9] imaged the ion beam exiting the quadrupole by photographing the phosphor of the position sensitive detector by recording individual events of the peak

Correspondence to: Ron M. A. Heeren; *e-mail:* heeren@amolf.nl

transition for *m/z* 219. A non-symmetrical cross-like distribution is observed at various positions across the peak. Birkinshaw et al. investigated focusing properties of ion beam exiting the QMS with and without electrostatic octopole lens [10]. A cross-like distribution with extremities pointing towards the QMS electrodes was observed when QMS was used without an octopole lens; when it was followed by an octopole lens, a circular distribution was observed. Some workers use monolayer films to image ion beam exiting the QMS and again a cross like distribution was observed [11]. Recently, Ferrer et al. studied the properties of ion beams of three different *m/z* ratios (28, 45, and 85 *m/z*) passing through a linear QMS with special attention to their dependence on the mass resolving power [12]. As expected significant losses in ion beam were observed at high resolution settings.

Much of the investigations reported in the literature were performed by considering the QMS as a residual gas analyzer and by adopting traditional theory for high vacuum environments; there are few exceptions where theoretical treatments of the radial ion density distribution in the collisional rf multipoles have been reported by taking into account the fast changing rf field, ion-neutral collisions, and ion–ion (space charge) interactions [13–16]. The phenomenon observed in [14, 15] was confirmed experimentally for collisional rf quadrupoles that are used both for external accumulation and as ion guides.

In vacuum pixel detectors that allow for position- [17, 18] and time-resolved [18–20] photoelectron and ion imaging have been increasingly used in the past few years in biological, biomolecular, and biomedical MS imaging (MSI). Previously, the use of the Timepix detector with other MS technologies such as secondary ion mass spectrometry (SIMS) [21] and a TOF instrument [22, 23] has been demonstrated for MSI with a spatial resolution of few micrometers. In this paper, the implementation of a Timepix detector system on a QMS with a cooling octopole ion guide is presented. The Timepix was employed to study the spatial distribution of mass-selected transmitted ions from a QMS. The detector was also used to study the transmission characteristics of different ion entrance conditions imparted via the octopole placed before the QMS, through the examination of the spatial distributions of the ions exiting the system.

Theory

QMS theory has been published in detail in [24]; however, it is reproduced here in brief for completeness. The QMS electrode assembly can operate either in mass selective ion transmission mode or high-pass mass filter mode (rf only) depending on applied voltages. When driven by the correct combination of DC and rf voltages, the QMS operates in mass selective ion transmission mode. With the voltage applied on the x electrodes $\varnothing_x$, and voltage applied on the y electrodes $\varnothing_y$ defined in Equations 1 and 2, the behavior of the ions as they pass through the QMS can be defined by the Mathieu Equation 3 [24].

$$\varnothing_x = (U - V\cos\omega t) \tag{1}$$

$$\varnothing_y = -(U - V\cos\omega t) \tag{2}$$

$$\frac{d^2u}{d\xi^2} + (a_u - 2q_u\cos(2\xi))u = 0 \tag{3}$$

Where V is the zero-to-peak amplitude of rf voltage oscillating with angular frequency ω (expressed in radians per second), U is the applied DC voltage, $u = x$ or y, ξ is a dimensionless modified time (t) parameter given by $\xi = \omega t / 2$, and *(a, q)* are the dimensionless stability parameters. The stability of solutions to Mathieu's equation when plotted in *a-q* space, results in overlapping transition curves representing regions of stability in two dimensions (x and y). This plot is commonly referred to as the Mathieu stability diagram [24, 25]. The stability parameters *(a, q)* are given by:

$$a_u = a_x = -a_y = \left(\frac{8eU}{mr_0^2\omega^2}\right) \tag{4}$$

$$q_u = q_x = -q_y = \left(\frac{-4eV}{mr_0^2\omega^2}\right) \tag{5}$$

where e is the charge on the ion in coulombs, m is the ion's mass, and r_0 is the inscribed QMS field radius. Under normal operating conditions, the mass filtering action of the QMS is controlled by electrode voltages U and V. The ratio of the voltages U and V controls the QMS resolution setting and the voltage V sets the mass scale.

When operated in rf only mode, the DC voltage is set to zero (i.e., $a = 0$) and the QMS is operated along the q axis of the stability diagram and the QMS acts as high-pass filter with the low mass cut off given by Equation 6 [26]:

$$M_{min} = \frac{4eV}{0.908\omega^2 r_0^2} \tag{6}$$

Experimental

The Medipix/Timepix Detectors

Developed by the Medipix collaboration and hosted by CERN (Medipix collaboration, www.cern.ch/medipix), the Medipix2 [27, 28]/Timepix [29] chips are active pixel detectors. The Medipix/Timepix family has found its way into high performance MS for imaging and diagnostic purposes of TOFMS instruments [22, 30]. Ions exiting the mass analyzer can be detected on Timepix chip by placing microchannel plates (MCPs) in front of the read-out chip [31]. Impact of ions on the MCPs produces electron showers, which are then detected by the readout chip. The dimension of an individual Medipix/

Timepix chip is 1.4 × 1.6 cm^2. The major characteristics of this application-specific integrated circuit (ASIC) are 256 × 256 pixels of 55 × 55 μm each per chip, low electronic noise, and pixel level functionality. In the work reported, we have employed an array of 2×2 Timepix chips.

In the Timepix chip, each pixel can be individually selected to operate in one of three modes: (1) the Medipix mode (i.e., the counting mode) in which each pixel counts the number of impinging particles; (2) the Timepix mode, in which the arrival time of one impinging particle is measured with respect to an external trigger/shutter signal; (3) the time-over-threshold (TOT) mode, in which the time is measured during which a fired pixel stays over a certain detection threshold. Different pixels can be operated in different modes. The chip is controlled via a dedicated acquisition and control software and graphical user interface, "Pixelman" [32]. In this investigation, all the results are produced using the Timepix chip operating in Medipix mode (the counting mode).

Mass Spectrometer

Figure 1a shows the 3D exploded view of the ESI octopole ion guide-quadrupole mass spectrometer (O-QMS) instrument setup; Figure 1b shows corresponding 2D schematic with visualization of different potentials used in the system. The MCP/Timepix detector, mounted on a vacuum flange, is placed inside the vacuum chamber 8 cm from the exit side of the quadrupole mass filter (QMF) (Quadrupole ABB Extrel; Extrel, Pittsburgh, PA, USA) as shown in Figure 1a. Ions are created by electrospray ionization (ESI). In all the experiments reported in this paper, the analyte was a 10 μM solution of bovine cytochrome *c* (Sigma Aldrich, Zwijndrecht, Netherlands) in 50/50 water/methanol (by volume) with 0.1% formic acid to aid protonation.

The octopole is used to interface the ESI ion source and the quadrupole mass spectrometer. The octopole has an electrode diameter of 6 mm, length 170.5 mm, and an inscribed field radius of 4.5 mm. The rf potential on octopole was maintained at 50 $V_{0\text{-peak}}$ and the rf was set at 1 MHz. The kinetic energy of ions entering the QMS will be influenced mainly by the DC bias applied to the octopole. Ions from the octopole travels into the quadrupole mass filter, which can either operate in transmission only mode (rf only mode) or mass-selective ion transmission mode. There is an ion lens assembly between the octopole and QMF, an exit electrode to the octopole, and an entrance electrode to QMF, which were all maintained at ground potential. The aperture diameter of both lens electrodes is 2 mm. The QMF has a mass range of up to 4000 *m/z*, a length of 210 mm, an electrode diameter of 9.525 mm, an inscribed field radius of ≈4.17 mm, and an operating frequency of 880 kHz. The pressure at the octopole section was 5.0 × 10^{-4} mbar and the operating pressure of the QMF section was 6.4 × 10^{-6} mbar.

A chevron MCP stack (F2225-21N290; Hamamatsu Photonics Deutschland GmbH, Herrschingam Ammersee, Germany; active area Φ = 4 cm, 12 μm pores, 15 μm pitch) is placed in front of the Timepix chip array. Ions exiting from the

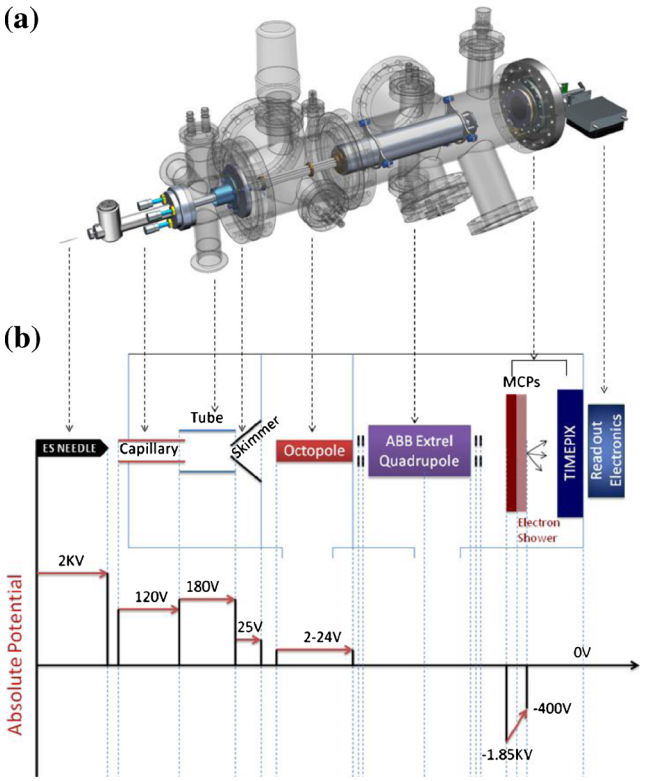

Figure 1. (**a**) 3D exploded view of the ESI based O-QMS instrument; (**b**) Corresponding 2D schematic presentation with visualization of absolute potential distribution of the system

quadrupole will impact on the MCPs and the resultant electron shower is projected on the Timepix chips. The front MCP was maintained at –1850 *V*, the back MCP at –400 V, and the Timepix detector was at ground potential. Timepix data is then acquired by the dedicated Pixelman software package. With this setting, for each ion impact 6 × 10^5 electrons are generated, which are projected on about four detector pixels. A detector pixel requires about 600 electron charges to register one count. This means that for one impacting ion, four pixels are activated, and the spatial resolution is then 0.1 mm. The Timepix detector accumulates data during an integration time of 100 ms and the accumulated data is then read out by the dedicated Pixelman software.

Data and image analysis were performed using software developed in Matlab-R2011b (Mathworks, Natick, MA, USA). The QMS assembly was controlled with the in-house developed AWG software [33], with a fully automated data acquisition electronic drive unit for scanning of the mass filter electrode voltages. To obtain a mass spectrum, the QMS scan steps and the Timepix integration/read-out times were synchronized. The scan rate of the QMF was set to a low value of 100 s across a mass range of 400–1400 Da. An acquisition time of 100 ms per frame was used and 1000 frames were recorded. The data of every measurement frame is saved in a separate sparse data file that contains the pixel address and the corresponding ion hits recorded by each pixel. Mass spectra are built by using the summed signals per frame. The spectrum is mass-

calibrated using the set mass range of the QMS. The settings, as described, are intended to give one integration point per 1 Da. It should also be noted that the QMS has mass resolution of approximately 2.3 Da full width at half maximum (FWHM). The *U/V* ratio was set at ≈0.168. The mass resolution is limited due to finite number of rf cycles the ion experiences in the quadrupole field.

Results and Discussion

Spatial Distribution of Ion Beam Exiting the ESI O-QMS

The QMS was operated in rf only mode and the amplitude of rf voltage was set to 1000 $V_{0\text{-peak}}$. With these settings, ions with *m/z* >800 are transmitted, allowing the dominant charge states of cytochrome *c* to pass through. The octopole DC bias voltage was set at 24 V. For every measurement, 200 Timepix frames were acquired and integrated with a 100 ms acquisition time per frame. Figure 2a shows the spatial distribution of the ion beam exiting the QMF as acquired by the Timepix. The projection of the ion beam on the detector has the shape of the slightly deformed ring. The ion intensity in the center of the beam is very low. It should also be noted that the diameter of the diverging beam on the Timepix detector is measured as ≈7.5 mm. Figure 2b shows the averaged radial intensity distribution with increasing radius from the center of the ion beam. To calculate the radial intensity distribution, concentric rings of one pixel on the Timepix chip with increasing radius are selected and the summed intensity of ions impacting the pixels on the concentric ring is calculated. It should be noted that the intensity distribution is normalized and smoothed using simple moving average (SMA) method.

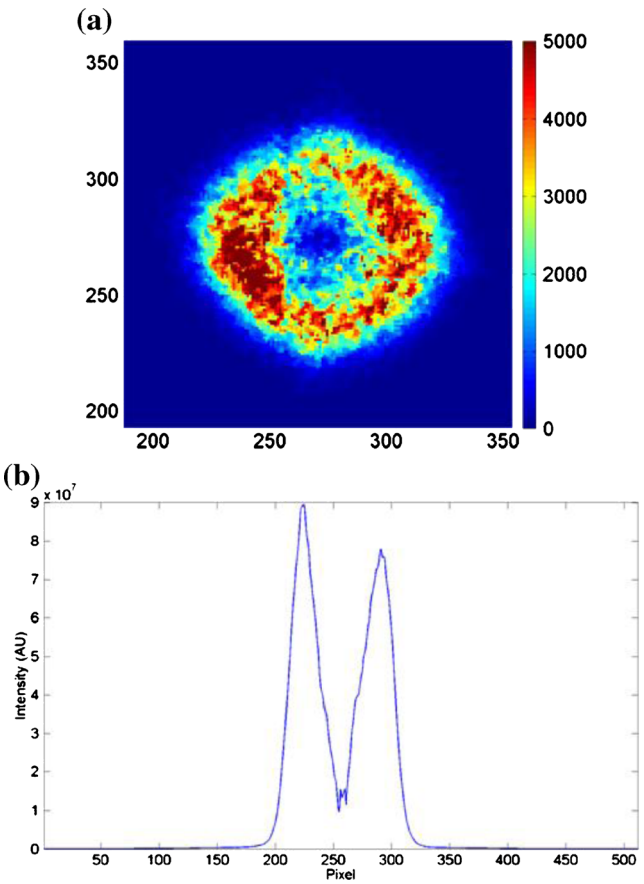

Figure 2. (**a**) Timepix measured ion beam spatial distribution of the O-QMS instrument operated in rf only mode; (**b**) Ion density distribution with increasing radius from the beam center

The result observed in Figure 2 is different from what you expect from a central introduction of ions in a QMS at a low *q* value, where ions might be expected to be concentrated around the central axis. At low *q* values, ion trajectories can make large excursions from the axis for several reasons. The most important parameters are the entrance conditions (e.g. x, y position and energy) and ion density leading to space charge effects. To a first approximation, at low *q* values, the amplitude of the ion motion in the QMS equals the x or y position at the entrance of the QMS. In this view, we conclude that the observed ion beam shape reflects the entrance conditions and that the beam shape is defined by the octopole and the space charge and/or hydrodynamics effects in the source region. It is well known that ion concentration on the axis is weak in an octopole, which can easily lead to a "ring"-shaped ion distribution exiting the octopole. This phenomenon was observed in computer simulations [15] for all multipoles and was confirmed experimentally for collisional rf quadrupoles used both for the external accumulation and as ion guides [34]. The theoretical treatment has also been reported in detail in the literature [14–16] where it is mentioned that under heavy loading conditions, the ions will have a radial distribution with a radius increasing with *m/z*.

Effect of DC Bias Applied to Octopole on Total Ion Transmission

The 2D ion distribution shown in Figure 2 was obtained with a bias voltage on the octopole of 24 V. An increase of octopole bias voltage from 2 to 24 V results first in a decrease of the total ion current followed by a gradual increase up to 24 V. This result is plotted in Figure 3. It should be noted that the ion current is expected to increase further with increase in DC bias voltage; however, the electronics is tuned to supply a maximum of 25 V. Furthermore, in Figure 3 the dependence of the ion beam spatial distribution as a function of the bias voltage is presented. Changing the bias voltage from 2 to 10 V leads to a decrease in beam diameter concomitant with a decrease in total ion current. Further increase in bias voltage from 10 to 24 V leads to an increase in beam diameter with an increase in total ion current.

The effect of the octopole bias voltage on the ion beam diameter and total transmitted ion current cannot be explained quantitatively. The voltage difference between octopole and QMS, in combination with the ion lens between the octopole

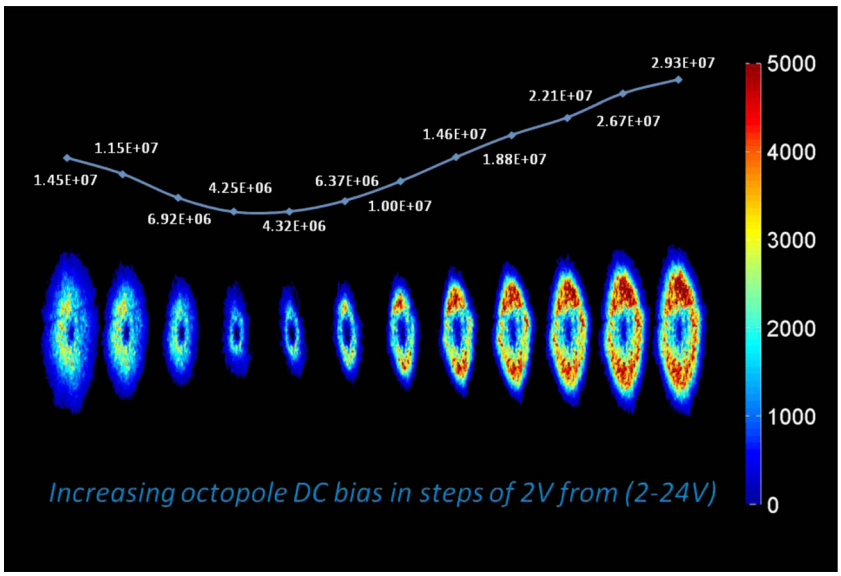

Figure 3. Experimentally measured effect of octopole DC bias potential on transmitted ion beam of rf only quadrupole, (top) total hits recorded on the Timepix, (bottom) spatial distribution of the ion beam

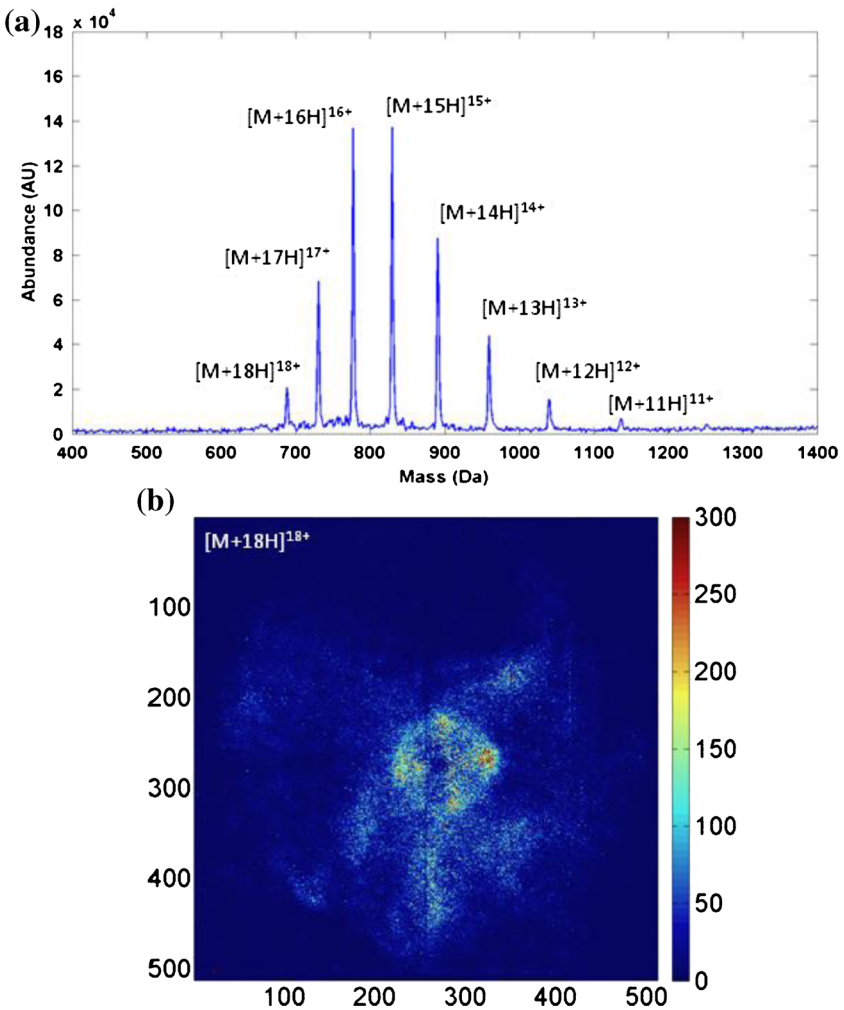

Figure 4. (**a**) Timepix generated ESI O-QMS mass spectrum of cytochrome *c*; (**b**) 2D spatial distribution of $[M + 18H]^{18+}$ charge state peak

and QMS, determine the ion injection parameters for the QMS, together with the RF fringe fields.

Spatial Distribution of Selected Ions Exiting the ESI O-QMS

Figure 4a shows an example ESI mass spectrum of the protein cytochrome *c* using the Timepix detector. The mass spectrum shows the charge state distribution, from $[M + 18H]^{18+}$ to $[M + 11H]^{11+}$. Figure 4b shows 2D spatial distribution of $[M + 18H]^{18+}$ charge state. The cross-like pattern obtained is comparable to the one observed by Weaver and Mathers [9]. It has to be noted that these distributions are recorded under selective ion transmission conditions, where the ion trajectories are close to their instability limit. This means that you can expect a large beam diameter. Furthermore, the radial velocity of the ions is very small in the vicinity of the quadrupole electrodes. This means that the chance to exit the QMS at positions towards the x- and y-electrodes is much larger (about five times) than leaving the QMS at the center. From the spatial information obtained the magnification of the beam from the exit lens of QMS was found to be approximately 2.5.

In an ideal situation, the spatial distribution of the ion beam exiting the QMS should be independent of *m/z* (e.g., for identical injection parameters) at the entrance of the QMS. However, since the cooling octopole ion guide is known to provide radial stratification of ions based on different *m/z* ratio, we have studied the radial distribution of different *m/z* ions of Figure 4a in detail. Figure 5a shows zoomed in 3D contour maps for each charge state. For better illustration of the radial distribution effect, we have zoomed in on the central intense area of the ion beam and the diameter of the zoomed in area is 7.5 mm. It should be noted that the distributions are normalized with respect to the intensity of $[M + 15H]^{15+}$. Furthermore, it has to be realized that the observed ion distribution depends critically on the proper setting of the QMS. Small deviations from the optimal rf and DC setting lead to differences in ion intensity distribution in the x-coordinate relative to the y-coordinate as a consequence of the change to the (a, q) coordinates of the ions. In Figure 5a the effects described above can be observed. The ion distributions show maxima on the regions close to the four electrodes axis and show a minimum at the center. For higher charge states 15+ to 18+ the ion intensity along the x-coordinate is visible. The lower charge states 11+ to 14+ have a very low intensity at the center.

Figure 5b shows the radial ion density distribution of different *m/z* charge states with increasing radius from the center of the ion cloud. An area of a pie-slice 315° to 25° along the positive x-coordinate was selected. It should also be noted that the ion density profile is smoothed using SMA, and normalized to the total ion count 1 with respect to the intensity of charge state 15+ for better illustration of the effect. The radial ion

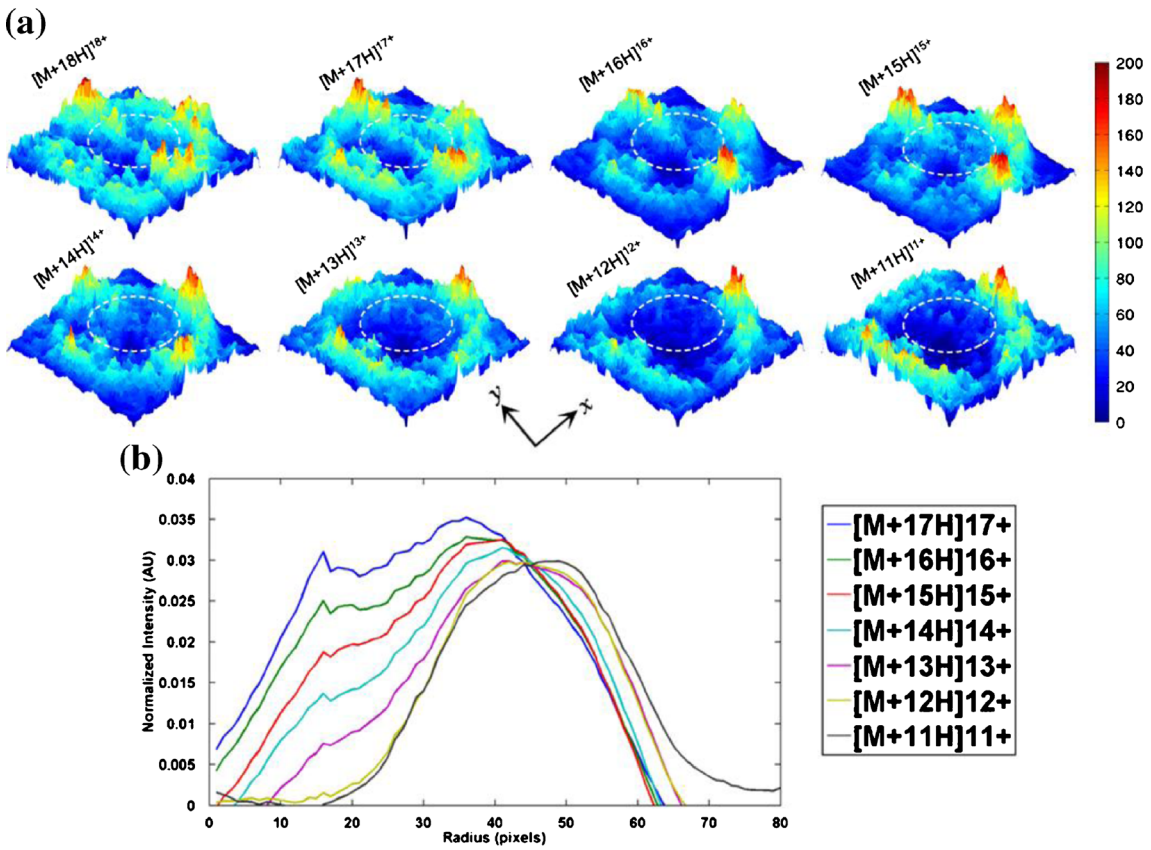

Figure 5. (**a**) Normalized 3D intensity contour maps of different charge states with reference circle (R = 30 pixels); (**b**) normalized radial ion density distribution for an ion beam consisting of several charge states of cytochrome *c*

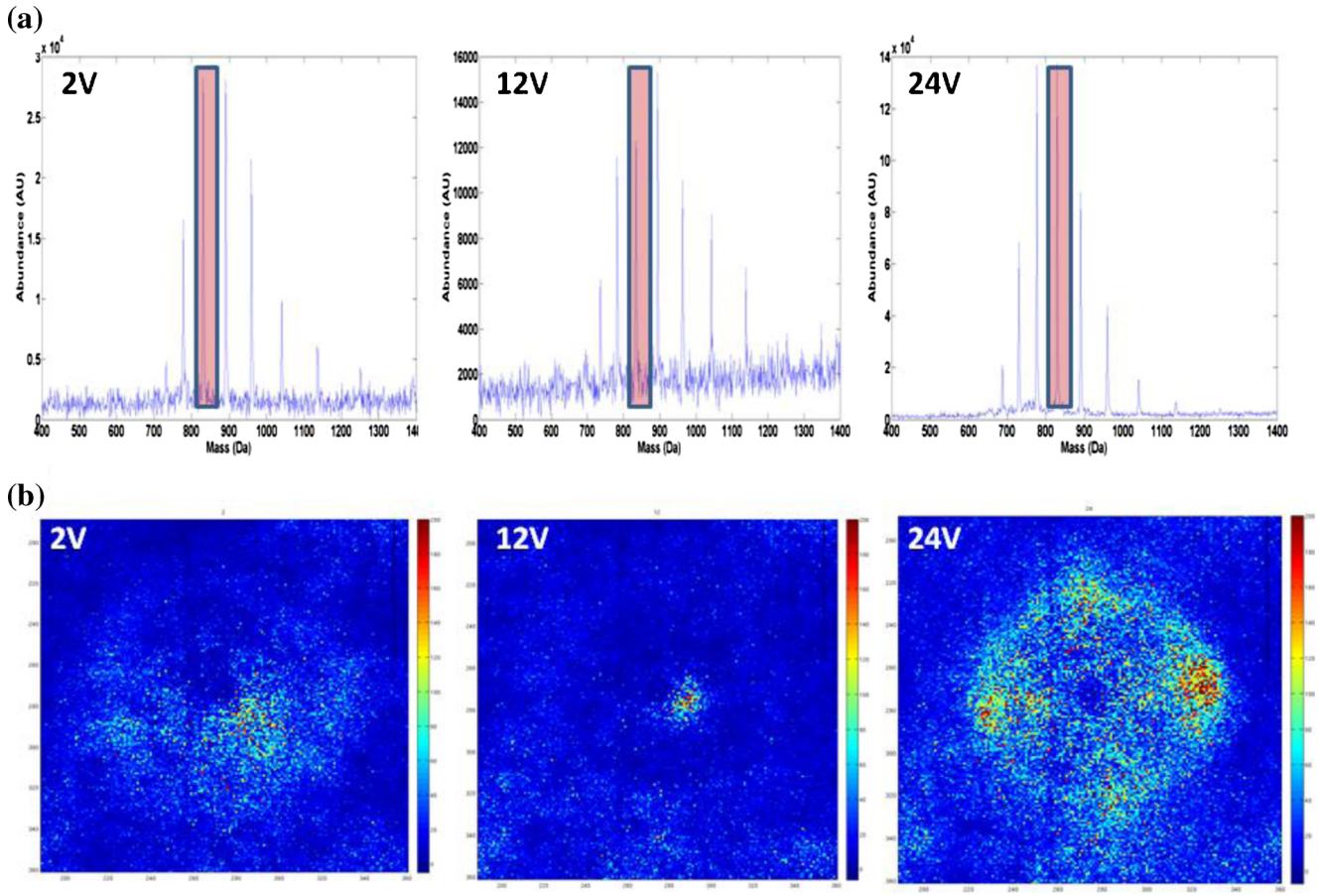

Figure 6. (**a**) Mass spectrum obtained at three different values of octopole DC bias: 2, 12, and 24 V; (**b**) corresponding spatial distribution of the peak highlighted in (**a**), $[M + 15H]^{15+}$

density distribution of different *m/z* values of cytochrome *c* clearly illustrates the change in radial distribution with increase in *m/z* ratio. The peak intensity shifts with increase in *m/z*. For the observed radial distribution the same explanations given for rf only mode with respect to the influence of exit beam distribution from octopole on exit beam profile of QMS stands true for selective ion transmission mode.

Effect of Octopole Bias Voltage on Selective Ion Transmission

Figure 6a shows mass spectra obtained at three different values of applied octopole DC bias (2, 12, and 24 V), and Figure 6b shows the corresponding spatial distribution of the highlighted mass peak (*m/z* = 820, $[M + 15H]^{15+}$).

The same trend as earlier observed for the total ion beam transmission was found for the transmission of the selected ions $[M + 15H]^{15+}$. From the obtained measurements, the intensity has a minimum at 10 V octopole bias voltage and a maximum at 24 V, and is expected to increase further with increase in bias voltage. The ratio of the ion intensities at bias voltages are comparable to the ratios observed for the total ion current transmissions presented in Figure 3. This is not surprising because the $[M + 15H]^{15+}$ ions constitute a major part of the total ion intensity.

Conclusions

A novel instrument consisting of a QMS coupled with a position-sensitive active pixel detector for imaging of ions exiting a QMS has been presented. Experimental studies using the developed instrument were performed to study the transmission characteristics of the QMS operated in both rf only and mass scanning mode.

The fundamental insight into ion motion observed with the help of the Timepix detector suggests that ion beam entrance conditions and entrance spatial distribution will have a direct impact on transmitted beam characteristics as expected. Also, our experimental findings confirm the predicted theoretical trends in literature for ESI-based instruments. Through this work, we have provided an unrivalled illustration of these well-known effects and with this new detector researchers can systematically investigate, visualize and directly measure the fine details of these points in a way and to accuracy that no previous researchers have been able to do so.

Acknowledgments

This work is part of the research program of the Foundation for Fundamental Research on Matter (FOM), which is part of the Netherlands Organization for Scientific Research (NWO). The research is supported by the Comprehensive Analytical Science and Technology (COAST) foundation, which is the assigned program committee in the NWO Technology Area for Sustainable Chemistry (TASC) program. The authors acknowledge Ronald Buijs, Marc Duursma, and Frans Giskes of AMOLF for their contribution to the experiments, and also Professor Stephen Taylor and Dr. Ken Evans of the University of Liverpool for their advice and constructive analysis during the course of this work.

References

1. Fenn, J.B., Mann, M., Meng, C.K., Wong, S.F., Whitehouse, C.M.: Electrospray ionization for mass spectrometry of large biomolecules. Science **246**(4926), 64–71 (1989)
2. Hang, W., Lewis, C., Majidi, V.: Practical considerations when using radio frequency-only quadrupole ion guide for atmospheric pressure ionization sources with time-of-flight mass spectrometry. Analyst **128**, 273–280 (2003)
3. Paul, W.: Das elektrische massenfilter. Z. Phys. **40**, 262–273 (1955)
4. Brubaker, W.M., Tuul, J.: Performance studies of a quadrupole mass filter. Rev. Sci. Instrum. **35**(8), 1007–1010 (1964)
5. Dylla, H.F., Jarrell, J.A.: Transmission-resolution curves for a quadrupole mass spectrometer with separated rf and DC fields in the entrance aperture. Rev. Sci. Instrum. **47**(3), 331–333 (1976)
6. Batey, J.H.: Quadrupole gas analyzers. Vacuum **37**, 659–668 (1987)
7. Konenkov, N.V.: Influence of fringing fields on the acceptance of a quadrupole mass filter in the separation mode of the intermediate stability region. Int. J. Mass Spectrom. Ion Process. **123**, 101–105 (1993)
8. Gibson, J.R., Evans, K.G., Syed, S.U., Maher, S., Taylor, S.: A method of computing accurate 3D fields of a quadrupole mass filter and their use for prediction of filter behavior. J. Am. Soc. Mass Spectrom. **23**, 1593–1601 (2012)
9. Price, E.D., Todd, J.F.J.: Dynamic Mass Spectrometry, Vol 5, pp. 41–54. Heyden and Son, London (1978)
10. Birkinshaw, K., Hirst, D.M., Jarrold, M.F.: The focusing of an ion beam from a quadrupole mass filter using an electrostatic octopole lens. Phys. E Sci. Instrum. **11**, 1037–1040 (1978)
11. Kane, T.E., Angelico, V.J., Wysocki, V.H.: Use of condensation figures to image low-energy ion beam damage of monolayer films. Anal. Chem. **66**, 3733–3736 (1994)
12. Ferrer, R., Kwiatkowski, A.A., Bollen, G., Lincoln, D.L., Morrissey, D.J., Pang, G.K., Ringle, R., Savory, J., Schwarz, S.: Ion beam properties after mass filtering with a linear radiofrequency quadrupole. Nucl. Inst. Methods Phys. Res. A **735**, 382–389 (2014)
13. Tolmachev, A.V., Udseth, H.R., Smith, R.D.: Charge capacity limitations of radio frequency ion guides in their use for improved ion accumulation and trapping in mass spectrometry. Anal. Chem. **72**, 970–978 (2000)
14. Tolmachev, A.V., Udseth, H.R., Smith, R.D.: Radial stratification of ions as a function of mass to charge ratio in collisional cooling radio frequency multipoles used as ion guides or ion traps. Rapid Commun. Mass Spectrom. **14**, 1907–1913 (2000)
15. Tolmachev, A.V., Udseth, H.R., Smith, R.D.: Modeling the ion density distribution in collisional cooling rf multipole ion guides. Int. J. Mass Spectrom. **222**, 155–174 (2000)
16. Grinfeld, D., Kopaev, I., Makarov, A., Monastyrskiy, M.: Space-charge effects in rf ion storage devices. ASMS, Colorado, USA (2011)
17. Gademann, G.H., Huismans, Y., Gijsbertsen, A., Jungmann, J., Visschers, J., Vrakking, M.J.J.: Velocity map imaging using an in-vacuum pixel detector. Rev. Sci. Instrum. **80**, 103105–103107 (2009)
18. Jungmann, J.H., MacAleese, L., Buijs, R., Giskes, F., de Snaijer, A., Visser, J., Visschers, J., Vrakking, M.J.J., Heeren, R.M.A.: Fast, high resolution mass spectrometry imaging using a Medipix pixelated detector. J. Am. Soc. Mass Spectrom. **21**(12), 2023–2030 (2010)
19. Jungmann, J.H., MacAleese, L., Visser, J., Vrakking, M.J.J., Heeren, R.M.A.: High dynamic range biomolecular ion microscopy with the Timepix detector. Anal. Chem. **83**(20), 7888–7894 (2011)
20. Bamberger, C., Renz, U., Bamberger, A.: Digital imaging mass spectrometry. J. Am. Soc. Mass Spectrom. **22**(6), 1079–1087 (2011)
21. Kiss, A., Jungmann, J.H., Smith, D.F., Heeren, R.M.A.: Microscope mode secondary ion mass spectrometry imaging with a Timepix detector. Rev. Sci. Instrum. **84**, 013704–7 (2013)
22. Jungmann, J.H., Smith, D.F., MacAleese, L., Klinkert, I., Visser, J., Heeren, R.M.A.: Biological tissue imaging with a position and time sensitive pixelated detector. J. Am. Soc. Mass Spectrom. **23**, 1679–1688 (2012)
23. Jungmann, J.H., Smith, D.F., Kiss, A., MacAleese, L., Buijs, R., Heeren, R.M.A.: An in-vacuum, pixelated detection system for mass spectrometric analysis and imaging of macromolecules. Int. J. Mass Spectrom. 341/342, 34–44 (2013)
24. Dawson, P.H.: Quadrupole Mass Spectrometry and Its Applications. Elsevier, Amsterdam (1976)
25. Douglas, D.J.: Linear quadrupoles in mass spectrometry. Mass Spectrom. Rev. **28**, 937–960 (2009)
26. Miller, P.E., Denton, M.B.: Transmission properties of rf-only quadrupole mass filter. Int. J. Mass Spectrom. Ion Process. **72**, 223–238 (1986)
27. Llopart, X.C., Dinapoli, M., Segundo, R.S., Pernigotti, D.E.: Medipix2, a 64 k pixel readout chip with 55 micron square elements working in single photon counting mode. IEEE Trans. Nucl. Sci. **49**, 2279–2283 (2002)
28. Llopart, X.C., Campbell, M.: First test measurements of a 64 k pixel readout chip working in single photon counting mode. Nucl. Inst. Methods A **509**, 157–163 (2003)
29. Llopart, X., Ballabriga, R., Campbell, M., Tlustos, L., Wong, W.: Timepix, a 65 k programmable pixel readout chip for arrival time, energy and/or photon counting measurements. Nucl. Inst. Methods Phys. Res. A **581**, 485–494 (2007)
30. Jungmann, J.H., Heeren, R.M.A.: Detection systems for mass spectrometry imaging—a perspective on novel developments with a focus on active pixel detectors. Rapid Commun. Mass Spectrom. **27**, 1–23 (2013)
31. Vallerga, J.M., Tremsin, J., Siegmund, A., Mikulec, O., Clark, B.A.: Optically sensitive Medipix2 detector for adaptive optics wavefront sensing. Nucl. Inst. Methods Phys. Res. A **546**, 263–269 (2005)
32. Turecek, D., Holy, T., Jakubek, J., Pospisil, S., Vykydal, Z.: Pixelman: a multi-platform data acquisition and processing software package for Medipix2, Timepix, and Medipix3 detectors. J. Instrum. **6**, pp. C01046 (2011). doi:10.1088/1748-0221/6/01/C01046
33. Barbu, I.T.M., van der Burgt, Y.E.M., Duursma, M.C., Takáts, Z., Seynen, M., Konijnenburg, M., Vijftigschild, A.J.M., Attema, I., Heeren, R.M.A.: A novel workflow control system for Fourier transform ion cyclotron resonance mass spectrometry allows for unique on-the-fly data-dependent decisions. Rapid Commun. Mass Spectrom. **22**, 1245–1256 (2008)
34. Tolmachev, A., Harkewicz, R., Alving, K., Masselon, C., Anderson, G., Rakov, V., Pasa-Tolic, L., Nikolaev, E., Belov, M., Udseth, H., Smith, R.D.: Radial stratification of ions as a function of *m/z* ratio in collisional cooling rf multipoles used as ion guides or ion traps. Proceedings of the 48th ASMS Conference, Long Beach, CA, June 11–15, p. 115 (CD ROM) (2000)